Coherent optical effects in a three-level quantum emitter near a periodic plasmonic nanostructure

Hamid R. Hamedi [1,*] Vassilios Yannopapas [2,†] Gediminas Juzeliūnas,[1,‡] and Emmanuel Paspalakis [3,§]

[1]*Institute of Theoretical Physics and Astronomy, Vilnius University, Saulėtekio 3, Vilnius LT-10257, Lithuania*

[2]*Department of Physics, National Technical University of Athens, Athens 157 80, Greece*

[3]*Materials Science Department, School of Natural Sciences, University of Patras, Patras 265 04, Greece*

(Received 20 November 2021; revised 8 July 2022; accepted 11 July 2022; published 21 July 2022)

We investigate optical effects in a three-level V-type quantum system involving two closely situated upper levels (a doublet), interacting with a weak probe field while located near a two-dimensional array of metal-coated dielectric nanospheres. We demonstrate that the presence of the plasmonic nanostructure leads to a significant modification of the absorption and dispersion properties of the quantum V system, yielding either very narrow resonances or induced transparency for the weak probe field. Introducing a weak incoherent pumping field can result in gain with and without population inversion in the quantum system, without the need for a strong coherent pump field. Such a gain can be controlled by varying the distance of the quantum system from the plasmonic nanostructure and by adjusting the amount of incoherent pumping, as well as the doublet splitting. The threshold limits are provided both analytically and numerically for achieving gain with and without inversion using the incoherent pumping. Our analysis paves the way toward further theoretical and experimental studies for mitigating dissipative losses in plasmonic modes when the gain is difficult to achieve due to impractical pumping requirements.

DOI: 10.1103/PhysRevB.106.035419

I. INTRODUCTION

Quantum coherence and interference in multilevel quantum systems near plasmonic nanostructures modify and eventually enhance the nonlinear optical effects at the nanoscale level, while at the same time introducing unexpected twists to numerous phenomena in mature subjects such as light-matter interactions and propagation of light [1,2]. Strong modification in nonlinear effects is mainly due to the large enhancement of the applied electric field, the strong exciton-plasmon coupling for quantum systems near plasmonic nanostructures, and the significant change of the spontaneous decay rate. A number of interesting effects has been investigated in this research area. Examples include the manipulation of spontaneous emission [3–10], optical transparency and slow light [11–14], refractive index enhancement [15] and modified two-photon absorption [16], Fano effects in energy absorption [17–20], controlled optical bistability [21–23], modification of the Kerr nonlinearity [24–26], four-wave mixing [27,28], tunable magneto-optical Faraday rotation [29], gain without inversion [30–34], controllable optically induced diffraction gratings [35,36], and many others [37–39].

Specifically, the concept of gain without population inversion holds promise for creating lasers in regimes where population inversion is hard to achieve. Different proposals have been put forward in the literature for the gain (and lasing) without inversion based on quantum interference between different transitions yielding amplification when the population inversion is absent [40–46]. The gain without population inversion has also been analyzed in a four-level double-V-type quantum system which interacts simultaneously with probe and pump laser fields and is located near a two-dimensional (2D) array of metal-coated dielectric nanospheres [34]. In such a four-level quantum system, one V-type transition is affected by the interaction with localized surface plasmons and this subsystem leads to quantum interference in spontaneous emission, while the other V subsystem interacts with free-space vacuum and with the external laser fields. Note that when such a system interacts with one or two weak probe laser fields in the transitions that are not affected by the localized surface plasmons, numerous appealing optical effects emerge including optical transparency and slow light [11], phase-dependent optical effects [12], gain without inversion [34], and controllable Kerr nonlinearities [26].

In this paper, we consider a V-type quantum system placed next to a plasmonic nanostructure. In this situation, the influence of the localized surface plasmons and the quantum interference effects happens in the same transitions of the quantum system that interact with the external laser field, and this, to the best of our knowledge, has not been explored so far. We focus on the influence of the coherent effects induced by the presence of the nanostructure on the absorption and dispersion properties of the emitter. In the proposed model the light-quantum system coupling, illustrated in Fig. 1(a), is similar to the one studied in Refs. [43,47], yet the presence of the plasmonic nanostructure substantially modifies the response of the system. We analyze the system in two different conditions: with and without the presence of the incoherent pumping. Applying a steady-state density-matrix analysis, we show that without the incoherent pumping field

*hamid.hamedi@tfai.vu.lt
†vyannop@mail.ntua.gr
‡gediminas.juzeliunas@tfai.vu.lt
§paspalak@upatras.gr

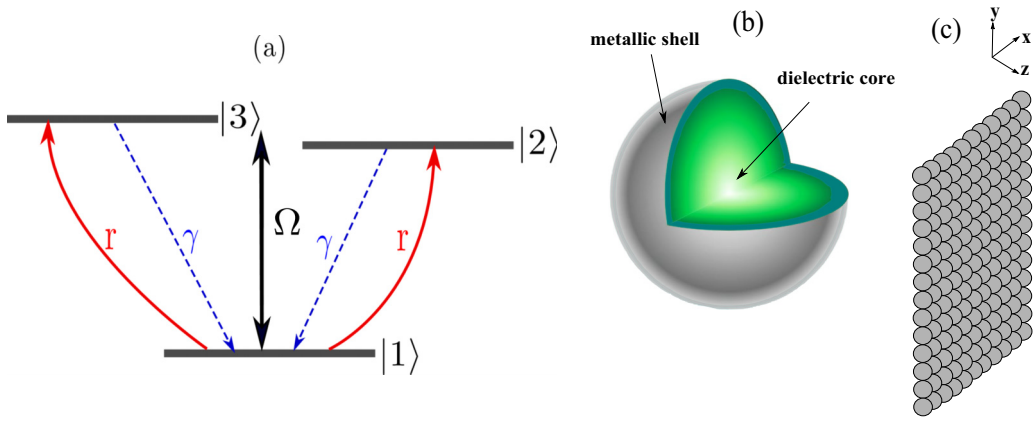

FIG. 1. Schematic diagram of the three-level quantum V system (a). A metal-coated dielectric nanosphere (b) and a 2D array of such spheres (c).

the plasmonic nanostructure induces either very narrow resonances or optical transparency. When the incoherent pumping is present, we observe the phenomena of gain with and without inversion which can be controlled by adjusting the rate of incoherent pumping, the distance of the quantum system from the plasmonic nanostructure, and the doublet splitting. While gain with inversion occurs even in the absence of plasmonic nanostructure, the inversionless gain can appear only when the quantum V system is next to the plasmonic nanostructure. We note that gain without inversion in a double-V-type system near the periodic plasmonic nanostructure has been studied in Ref. [34], but in that case the quantum interference effects in spontaneous emission and the coupling of the laser fields occurred in different V-type subsystems and also the creation of gain without inversion required the addition of a moderate to strong coherent (laser) field in addition to the probe field, while here only an incoherent pumping field is applied in addition to the probe field.

II. MODEL

A. Hamiltonian

We analyze the light-matter interaction in a three-level quantum V-type system with two closely lying upper states $|2\rangle$ and $|3\rangle$, as well as a lower state $|1\rangle$ shown in Fig. 1(a). For the V-type three-level system, one may consider either atoms, molecules, or quantum dots, where the V-type energy configuration is one of the basic energy configurations for coherent light-matter interactions. The quantum system is placed in vacuum and at distance d from the surface of the plasmonic nanostructure [Fig. 1(b)]. The upper states $|2\rangle$ and $|3\rangle$ represent two Zeeman sublevels ($J = 1, M_J = \pm 1$), while the lower state $|1\rangle$ corresponds to a level with $J = 0$, such that

$$\overrightarrow{\mu} = \mu(|2\rangle\langle 1|\hat{\varepsilon}_- + |3\rangle\langle 1|\hat{\varepsilon}_+) + \text{H.c.} \tag{1}$$

denotes the dipole moment operator. Here, the right-rotating ($\hat{\varepsilon}_+$) and left-rotating ($\hat{\varepsilon}_-$) unit vectors are defined by $\hat{\varepsilon}_\pm = (\mathbf{e}_z + i\mathbf{e}_x)/\sqrt{2}$, and μ is taken to be real.

The quantum system interacts with a linearly polarized continuous-wave electromagnetic laser field characterized by an electric-field component $\overrightarrow{E}(t) = \hat{z}E_0\cos(\omega t)$, where E_0 is the electric field amplitude and ω is its angular frequency. The laser field induces transitions between the state $|1\rangle$ and the states $|2\rangle$ and $|3\rangle$. Applying the dipole and rotating-wave approximations, the Hamiltonian describing the coupling of the laser field with the quantum V system is given by

$$H = \hbar\Big(-\delta - \frac{\omega_{32}}{2}\Big)|2\rangle\langle 2| + \hbar\Big(-\delta + \frac{\omega_{32}}{2}\Big)|3\rangle\langle 3| - \frac{\hbar\Omega}{2}(|1\rangle\langle 2| + \text{H.c.}), \tag{2}$$

where $\delta = \omega - \tilde{\omega}$ is the detuning of the applied electromagnetic field from the frequency $\tilde{\omega} = (\omega_2 + \omega_3)/2 - \omega_0$, the latter $\tilde{\omega}$ representing the difference between the average transition energy of the excited states $|2\rangle$ and $|3\rangle$ and that of the ground state $|1\rangle$. Here also $\Omega = \mu E_0\sqrt{2}\hbar$ is the Rabi frequency of the laser field, $\hbar\omega_n$ is the energy of the state $|n\rangle$, and $\omega_{32} = (\omega_3 - \omega_2)/2$. Both upper states $|2\rangle$ and $|3\rangle$ decay spontaneously to the ground state $|1\rangle$ with decay rates $2\gamma_2$ and $2\gamma_3$, respectively. The frequencies of transitions from the states $|2\rangle$ and $|3\rangle$ to $|1\rangle$ lie within the surface-plasmon resonance bands of the plasmonic nanostructure. Two incoherent pumping fields r_1 and r_2 ($r_1 = r_2 = r$) pump populations from the lower state $|1\rangle$ to excited states $|2\rangle$ and $|3\rangle$, playing the role of a one-way pump process. We also define Γ_0 as the decay rate of states $|2\rangle$ and $|3\rangle$ to state $|1\rangle$ in the vacuum, and take $\gamma_2 = \gamma_3 = \gamma$ [11].

B. Equations of motion and plasmonic nanostructure

Assuming a Markovian response, the following equations can be obtained for the density matrix elements of the quantum system described by the Hamiltonian of Eq. (2):

$$\dot{\rho_{21}} = \Big(i\delta + \frac{i\omega_{32}}{2} - \gamma - \gamma_{21} - r\Big)\rho_{21} - i\frac{\Omega}{2}\rho_{22} - i\frac{\Omega}{2}\rho_{23} + i\frac{\Omega}{2}\rho_{11} - \kappa\rho_{31}, \tag{3}$$

$$\dot{\rho_{31}} = \Big(i\delta - \frac{i\omega_{32}}{2} - \gamma - \gamma_{31} - r\Big)\rho_{31} - i\frac{\Omega}{2}\rho_{33} - i\frac{\Omega}{2}\rho_{32} + i\frac{\Omega}{2}\rho_{11} - \kappa\rho_{21}, \tag{4}$$

$$\dot{\rho_{23}} = (i\omega_{32} - 2\gamma - \gamma_{23})\rho_{23} + i\frac{\Omega}{2}\rho_{13} - i\frac{\Omega}{2}\rho_{21} - \kappa(\rho_{22} + \rho_{33}), \tag{5}$$

$$\dot{\rho_{22}} = -2\gamma\rho_{22} + r\rho_{11} + i\frac{\Omega}{2}(\rho_{12} - \rho_{21}) - \kappa(\rho_{23} + \rho_{32}), \tag{6}$$

$$\dot{\rho_{33}} = -2\gamma\rho_{33} + r\rho_{11} + i\frac{\Omega}{2}(\rho_{13} - \rho_{31}) - \kappa(\rho_{23} + \rho_{32}), \tag{7}$$

subject to the population conservation law $\rho_{11} + \rho_{22} + \rho_{33} = 1$ and $\rho_{ij} = \rho_{ji}^*$. In the above equations, γ_{ij} are the dephasing rates. Moreover, the parameter κ is the coupling coefficient between the states $|2\rangle$ and $|3\rangle$ due to spontaneous emission in a modified anisotropic vacuum [48], which is responsible for the emergence of quantum interference [49].

The values of γ and κ are given by [3,50–53]

$$\gamma = \frac{\mu_0\mu^2\bar{\omega}^2}{2\hbar}\hat{\varepsilon}_- \cdot \mathrm{Im}\,\mathbf{G}(\mathbf{r}, \mathbf{r}; \bar{\omega}) \cdot \hat{\varepsilon}_+, \tag{8}$$

$$\kappa = \frac{\mu_0\mu^2\bar{\omega}^2}{2\hbar}\hat{\varepsilon}_+ \cdot \mathrm{Im}\,\mathbf{G}(\mathbf{r}, \mathbf{r}; \bar{\omega}) \cdot \hat{\varepsilon}_+. \tag{9}$$

Here, $\mathbf{G}(\mathbf{r}, \mathbf{r}; \bar{\omega})$ [$\bar{\omega} = (\omega_3 + \omega_2)/2 - \omega_1$] is the dyadic electromagnetic Green's tensor, and $\mathbf{r}$ and μ_0 stand for the position of the quantum emitter and the permeability of vacuum, respectively. Calling on Eqs. (8) and (9), one can find the values of γ and κ as [3,50–53]

$$\gamma = \frac{\mu_0\mu^2\bar{\omega}^2}{2\hbar}\,\mathrm{Im}[G_\perp(\mathbf{r}, \mathbf{r}; \bar{\omega}) + G_\parallel(\mathbf{r}, \mathbf{r}; \bar{\omega})] = \frac{1}{2}(\Gamma_\perp + \Gamma_\parallel), \tag{10}$$

$$\kappa = \frac{\mu_0\mu^2\bar{\omega}^2}{2\hbar}\,\mathrm{Im}[G_\perp(\mathbf{r}, \mathbf{r}; \bar{\omega}) - G_\parallel(\mathbf{r}, \mathbf{r}; \bar{\omega})] = \frac{1}{2}(\Gamma_\perp - \Gamma_\parallel). \tag{11}$$

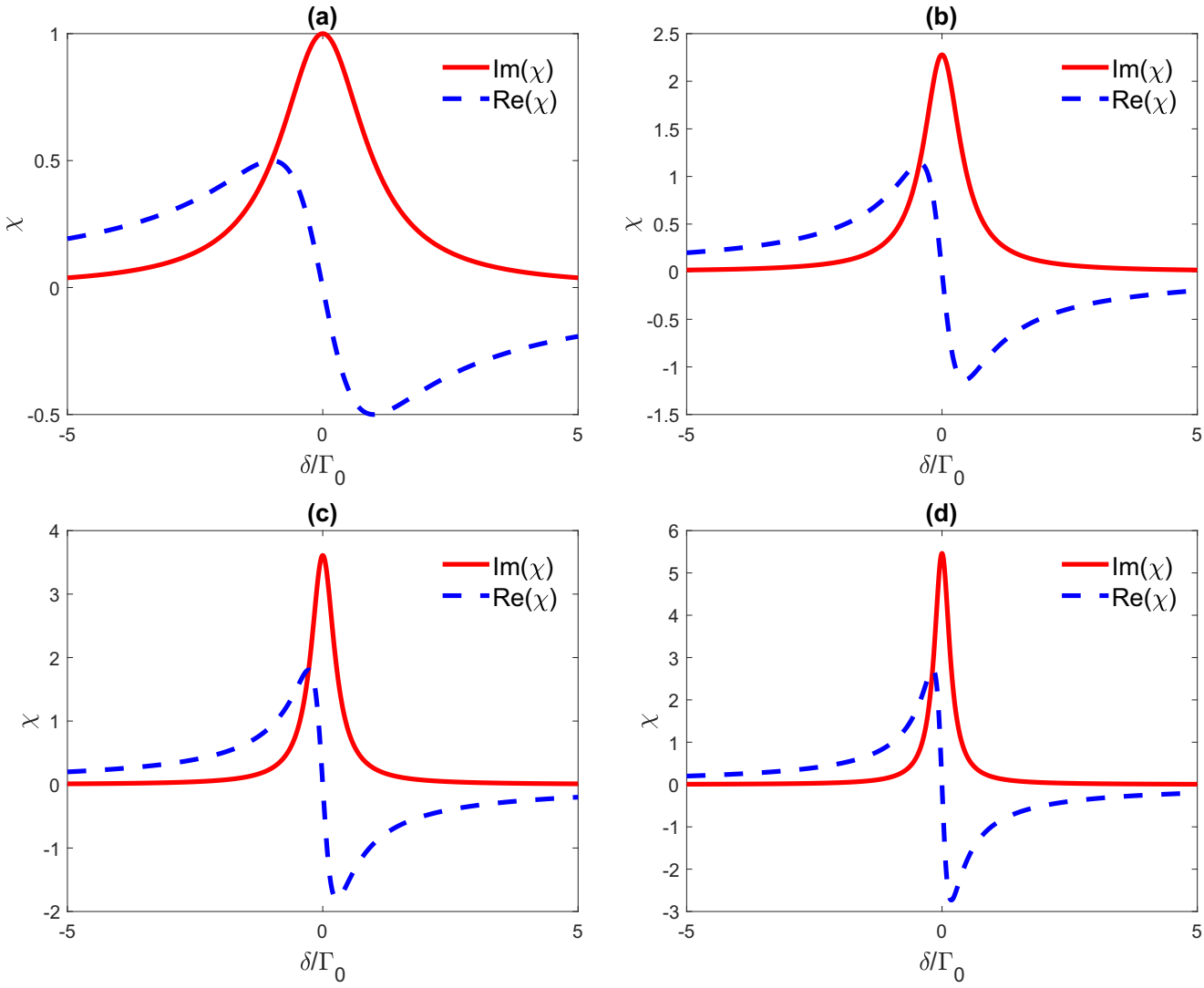

FIG. 2. The absorption spectrum [Im(χ); solid curve] and dispersion spectrum [Re(χ); dashed curve] of the quantum V system for the weak probe field Ω in units of $\frac{N\mu^2}{\varepsilon_0\hbar}$ as a function of the probe detuning δ. (a) is in the absence of the plasmonic nanostructure ($d = \infty$), while (b), (c), and (d) are in the presence of the plasmonic nanostructure. We take here $\omega_{32} = 0$, $r = 0$. In (a), the decay rate is Γ_0, but in (b)–(d) $\bar{\omega} = 0.632\omega_p$. In (b)–(d), the distance d of the quantum system from the plasmonic nanostructure is (b) $d = 0.8c/\omega_p$, (c) $d = 0.9c/\omega_p$, and (d) $d = c/\omega_p$.

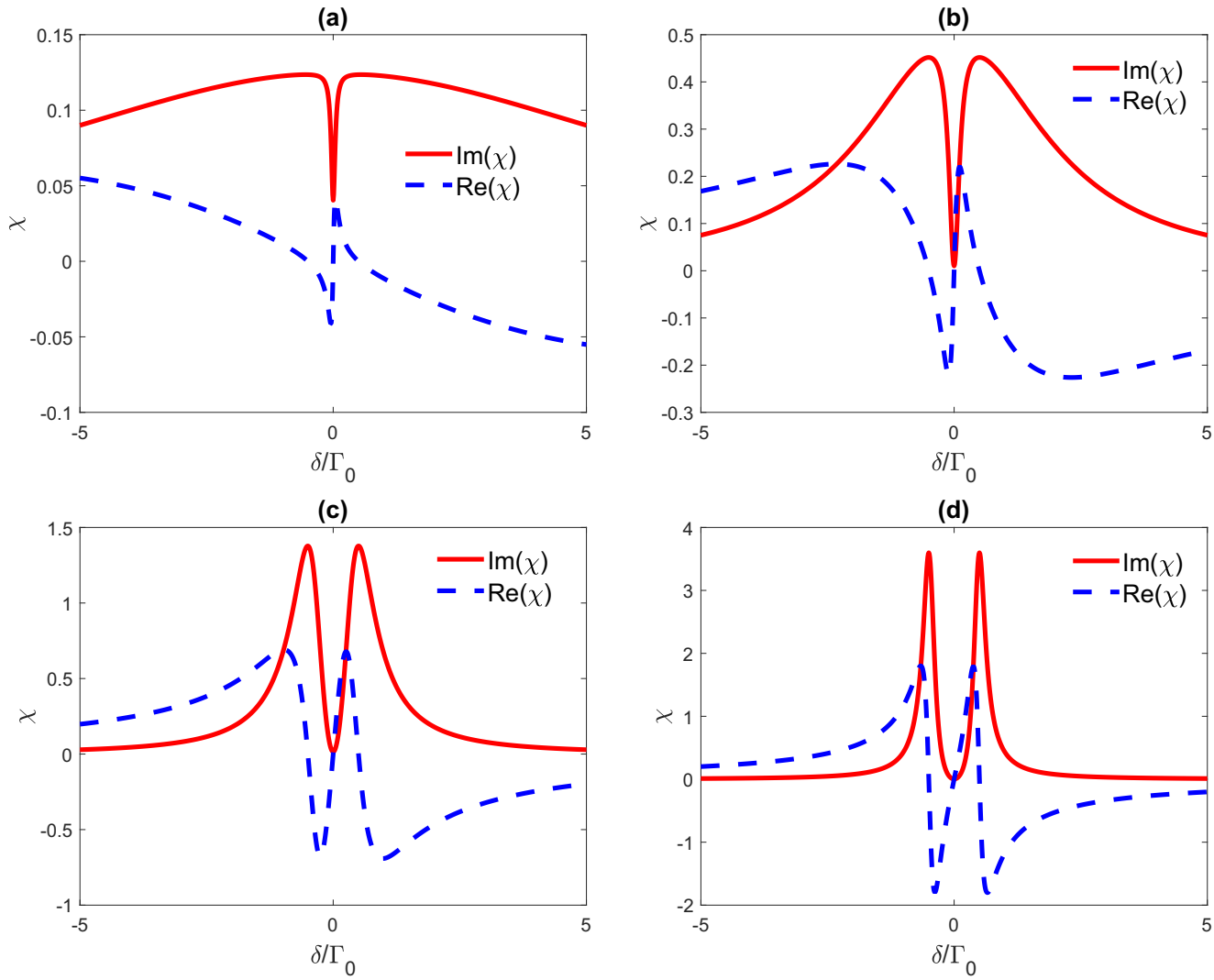

FIG. 3. The absorption spectrum [Im(χ); solid curve] and dispersion spectrum [Re(χ); dashed curve] of the quantum V system for the weak probe field Ω in units of $\frac{N\mu^2}{\varepsilon_0\hbar}$ as a function of the probe detuning δ. We take here $\omega_{32} = \Gamma_0$, $r = 0$, $\bar{\omega} = 0.632\omega_p$. In (a)–(d), the distance d of the quantum system from the plasmonic nanostructure is (a) $d = 0.3c/\omega_p$, (b) $d = 0.5c/\omega_p$, (c) $d = 0.7c/\omega_p$, and (d) $d = 0.9c/\omega_p$.

Here $G_\perp(\mathbf{r}, \mathbf{r}; \bar{\omega}) = G_{zz}(\mathbf{r}, \mathbf{r}; \bar{\omega})$ and $G_\parallel(\mathbf{r}, \mathbf{r}; \bar{\omega}) = G_{xx}(\mathbf{r}, \mathbf{r}; \bar{\omega})$ are the components of the electromagnetic Green' s tensor; the symbols $\perp$ and $\parallel$ refer to a dipole oriented, respectively, normal (along the z axis) and parallel (along the x axis) to a given structure which is of plasmonic nature in our case. The spontaneous emission rate is for an emitter oriented normal and parallel to the surface: $\Gamma_{\perp,\parallel} = \mu_0\mu^2\bar{\omega}^2\,\mathrm{Im}[G_{\perp,\parallel}(\mathbf{r}, \mathbf{r}; \bar{\omega})]/\hbar$. The corresponding degree of quantum interference is defined as

$$p = (\Gamma_\perp - \Gamma_\parallel)/(\Gamma_\perp + \Gamma_\parallel). \tag{12}$$

The value $|p| = 1$ corresponds to the maximum degree of quantum interference in the spontaneous emission [49]. This usually occurs when the emitter is placed in proximity to the structure that can completely quench $\Gamma_\perp$. On the other hand, when the emitter lies in the free-space vacuum, one has $\Gamma_\perp = \Gamma_\parallel$ giving $\kappa = 0$ and thus $p = 0$, so the quantum interference is completely absent in the V-type system.

The plasmonic nanostructure considered in the present work is a 2D square lattice of touching metal-coated silica nanospheres [Figs. 1(b) and 1(c)]. The periodic array of such nanoshells can be realized via self-assembly [54] and nanopatterning and nanolithographic [55,56] techniques.

The dielectric function of the metallic nanoshell is provided by a Drude-type electric permittivity

$$\epsilon(\omega) = 1 - \frac{\omega_p^2}{\omega(\omega + i/\tau)}, \tag{13}$$

where ω_p and τ are the bulk plasma frequency and the relaxation time of the conduction-band electrons of the metal, respectively. We note that the above generic model for the dielectric function of gold allows for adopting dimensionless units for the physical parameters involved, which renders our results applicable to other materials described by the Drude-type dielectric function such as the other noble metals or doped semiconductors with response in the IR region. The

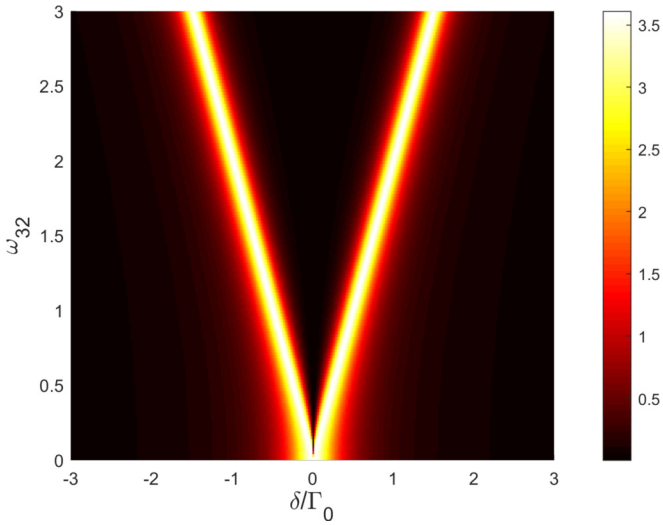

FIG. 4. The absorption spectrum [Im(χ)] of the quantum V system for the weak probe field Ω in units of $\frac{N\mu^2}{\varepsilon_0\hbar}$ as a function of the probe detuning δ and ω_{32}. We take here $r = 0$, $\bar{\omega} = 0.632\omega_p$, and $d = 0.9c/\omega_p$.

adoption of a more comprehensive experimental dielectric function, such as that of Ref. [57], containing the contribution of interband transitions is an unnecessary complication to our study since we are not interested in exploring a wide region in the visible/UV regime. We merely focus our study on a narrow window around a surface-plasmon resonance of the gold nanoshell in which case the interband transitions are spectrally distinct from this resonance and do not influence our results.

A typical value of the plasma frequency for gold is $\hbar\omega_p = 8.99$ eV [58,59]. This also determines the length scale of the system as $c/\omega_p \approx 22$ nm. The dielectric constant of SiO_2 is taken to be $\epsilon = 2.1$. In all the calculations that follow, we have assumed that $\tau^{-1} = 0.05\omega_p$. The lattice constant of the square array is $a = 2c/\omega_p$. The geometry of nanoshells is described by the total sphere radius $S = c/\omega_p$ and the core radius $S_c = 0.7c/\omega_p$.

The electromagnetic Green' s tensor providing the corresponding spontaneous emission rates $\Gamma_\perp$ and $\Gamma_\parallel$ is given by [3,60,61]

$$G^{EE}_{ii'}(\mathbf{r},\mathbf{r};\bar{\omega}) = g^{EE}_{ii'}(\mathbf{r},\mathbf{r};\omega) - \frac{i}{8\pi^2}\iint_{SBZ} d^2\mathbf{k}_\parallel \sum_{\mathbf{g}} \frac{1}{c^2 K^+_{\mathbf{g};z}} \times \nu_{\mathbf{gk}_\parallel;i}(\mathbf{r}) \exp(-i\mathbf{K}^+_{\mathbf{g}}\cdot\mathbf{r})\hat{\mathbf{e}}_{i'}(\mathbf{K}^+_{\mathbf{g}}), \quad (14)$$

with

$$\nu_{\mathbf{gk}_\parallel;i}(\mathbf{r}) = \sum_{\mathbf{g}'} R_{\mathbf{g}';\mathbf{g}}(\omega,\mathbf{k}_\parallel)\exp(-i\mathbf{K}^-_{\mathbf{g}'}\cdot\mathbf{r})\hat{\mathbf{e}}_i(\mathbf{K}^-_{\mathbf{g}'}) \quad (15)$$

and

$$\mathbf{K}^\pm_{\mathbf{g}} = \{\mathbf{k}_\parallel + \mathbf{g}' \pm [q^2 - (\mathbf{k}_\parallel + \mathbf{g})^2]^{1/2}\}, \quad (16)$$

where $\mathbf{g}$ are the reciprocal-lattice vectors corresponding to the 2D periodic lattice of the plane of scatterers, while $\mathbf{k}_\parallel$ is the reduced wave vector lying within the surface Brillouin zone associated with the reciprocal lattice of the spheres [62,63]. When $q^2 = \omega^2/c^2 < (k_\parallel + \mathbf{g})^2$, the wave vector $\mathbf{K}^\pm_{\mathbf{g}}$ has an imaginary part, so one arrives at an evanescent wave. The term $g^{EE}_{ii'}(\mathbf{r},\mathbf{r};\omega)$ in Eq. (14) is the free-space Green' s tensor and $\hat{\mathbf{e}}_i(\mathbf{K}^\pm_{\mathbf{g}})$ is the polar unit vector normal to $\mathbf{K}^\pm_{\mathbf{g}}$. Here also $R_{\mathbf{g}';\mathbf{g}}(\omega,\mathbf{k}_\parallel)$ denotes the reflection matrix, which provides a sum (over $\mathbf{g}$' s) of reflected (diffracted) beams generated by the incidence of a plane wave from the left of the plane of scatterers [62,63]. Also, in Eq. (14) the terms corresponding to s-polarized waves [those containing components with the unit vector $\hat{\mathbf{e}}_i(\mathbf{K}^\pm_{\mathbf{g}})$ normal to $\mathbf{K}^\pm_{\mathbf{g}}$] make a trivial contribution to the total decay rates and thus have been neglected.

About the calculation of the electromagnetic (EM) Green's tensor, we note that in each plane of particles, the method calculates the full multipole expansion of the total multiply scattered wave field and deduces the corresponding transmission and reflection matrices in the plane wave basis. As a full-multipole EM solver, there is no theoretical restriction in the size of the particles as is the case in methods operating in the dipole approximation or in similar long-wavelength approximations. Furthermore, our method has been recently extended to treat nonspherical scatters such as nanocubes and nanoprisms [64]; its chief advantage over mainstream commercial EM solvers lies in the fact that it can treat accurately and efficiently in terms of CPU time finite slabs of metamaterials/nanostructures, i.e., slabs containing many planes of scatterers thanks to the use of scattering matrices (transmission/reflection) for each plane of scatterers.

We take $\bar{\omega} = 0.632\omega_p$, and introduce d as the distance between the quantum system and the surface of the plasmonic nanostructure (plane of sphere centers). For the values of $\Gamma_\perp$ and $\Gamma_\parallel$ associated with different distances to the plasmonic nanostructure employed in the present work, we refer to Fig. 3 in Ref. [11]. It is found that $\Gamma_\parallel$ undergoes significant suppression and its actual value becomes much smaller than the corresponding free-space decay rate. Furthermore, the value of $\Gamma_\perp$ decreases as we increase the distance between the quantum emitter and the plasmonic nanostructure. When the quantum emitter is placed very close to the lattice of the plasmonic nanoshells, $\Gamma_\perp$ becomes much larger than the free-space decay rate. The value of $\Gamma_\perp$ is larger than the decay rate in vacuum for distances up to $0.6c/\omega_p$. However, for separations between $0.65c/\omega_p$ and c/ω_p, the decay rate $\Gamma_\perp$ is lower than that in the vacuum.

III. RESULTS AND ANALYSIS

A. Electric susceptibility

The electric susceptibility of the system characterizing the absorption and dispersion properties of the weak probe field is defined by

$$\chi(\delta) = \frac{\sqrt{2}N\mu}{\varepsilon_0 E_0}(\rho_{21} + \rho_{31}) = \frac{N\mu^2}{\varepsilon_0\hbar}\frac{\rho_{21} + \rho_{31}}{\Omega}, \quad (17)$$

where ρ_{21} and ρ_{31} are the steady-state solutions of the density matrix equations (3)–(7). Here, ε_0 is the vacuum permittivity and N is the density of the quantum emitters.

Using Eqs. (3)–(7), one has ($\gamma_{ij} = 0$)

$$\rho_{21} + \rho_{31} = i\frac{\Omega}{2}\frac{[(X+\kappa)(\rho_{33}-\rho_{11}) + (Y+\kappa)(\rho_{22}-\rho_{11})] + [\rho_{32}(\kappa+X) + \rho_{23}(\kappa+Y)]}{XY-\kappa^2}, \tag{18}$$

where $X = [i\delta + \frac{i\omega_{32}}{2} - \gamma - r]$ and $Y = [i\delta - \frac{i\omega_{32}}{2} - \gamma - r]$.

Here ρ_{jj} ($j = 1, 2, 3$) is the steady-state population of the level $|j\rangle$, while

$$\rho_{23} = \rho_{32}^{*} = \frac{\kappa(\rho_{22}+\rho_{33})}{i\omega_{32} - 2\gamma} \tag{19}$$

are the coherence terms induced by quantum interference.

Equation (18) consists of two parts. The first term stems from the direct transitions $|1\rangle \to |2\rangle$, $|1\rangle \to |3\rangle$ and depends on the population inversions ($\rho_{ii} - \rho_{11}$) ($i = 2, 3$). The second term (proportional to the coherence terms ρ_{32} and ρ_{23}) is due to the emergence of the quantum interference when the system is placed near the plasmonic nanostructure. The latter interference plays an important role in creating optical transparency in the quantum system and, as we will show later, enables creation of inversionless gain.

B. Absorption (gain) and dispersion properties

1. Without incoherent pumping

We start with the analysis of the effects of the plasmonic nanostructure on the absorption [Im(χ)] and dispersion [Re(χ)] spectrum of the quantum V system in the absence of incoherent pumping. Note that in our notation, absorption is obtained when Im(χ) > 0 while gain appears when

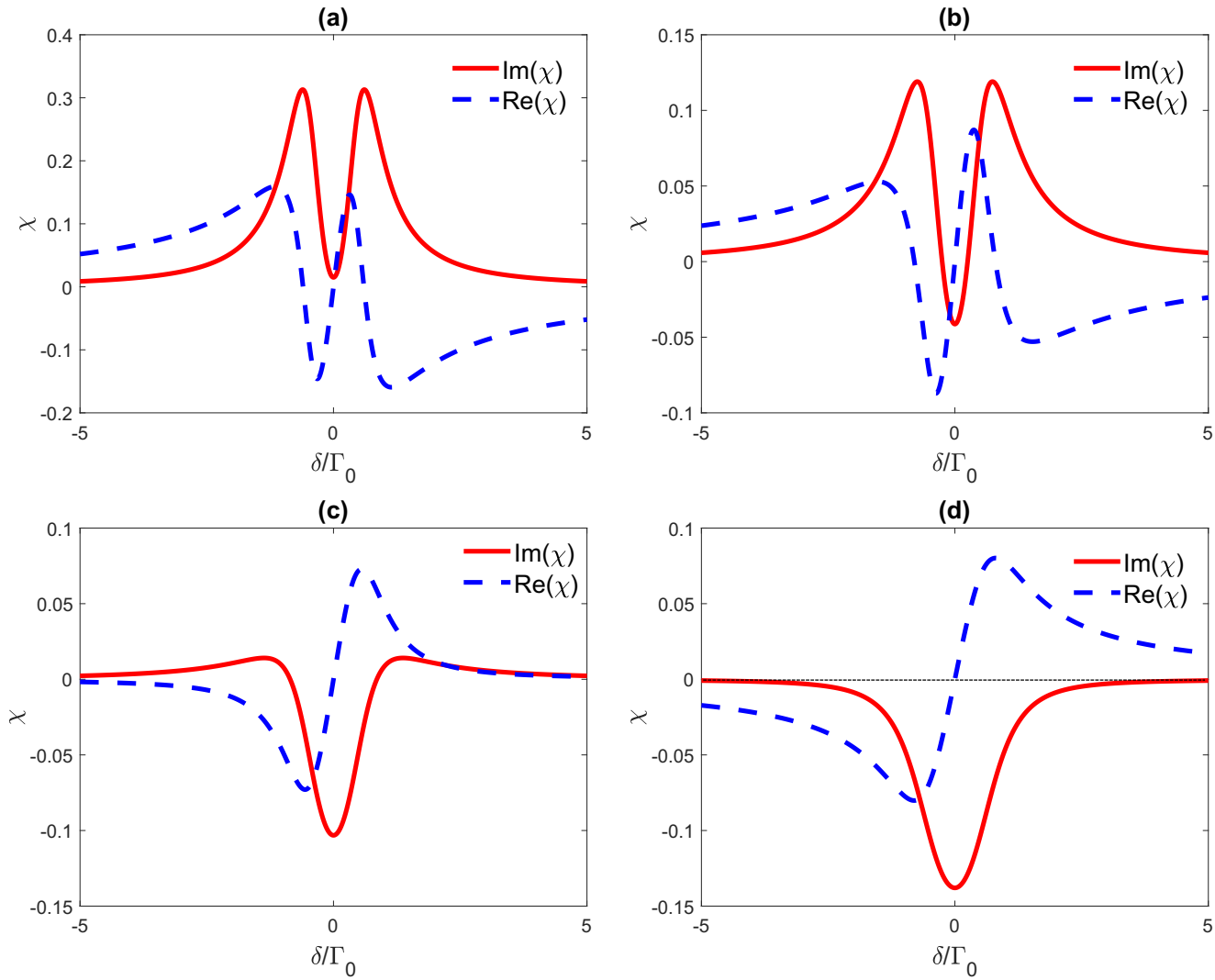

FIG. 5. The absorption (gain) spectrum [Im(χ); solid curve] and dispersion spectrum [Re(χ); dashed curve] of the quantum V system for the weak probe field Ω in units of $\frac{N\mu^2}{\varepsilon_0\hbar}$ as a function of the probe detuning δ. We take here $\omega_{32} = \Gamma_0$, $\bar{\omega} = 0.632\omega_p$, $d = 0.8c/\omega_p$. In (a)–(d), the incoherent pumping rate is (a) $r = 0.2\Gamma_0$, (b) $r = 0.3\Gamma_0$, (c) $r = 0.45\Gamma_0$, and (d) $r = 0.6\Gamma_0$. The horizontal dotted line indicates the zero-absorption limit.

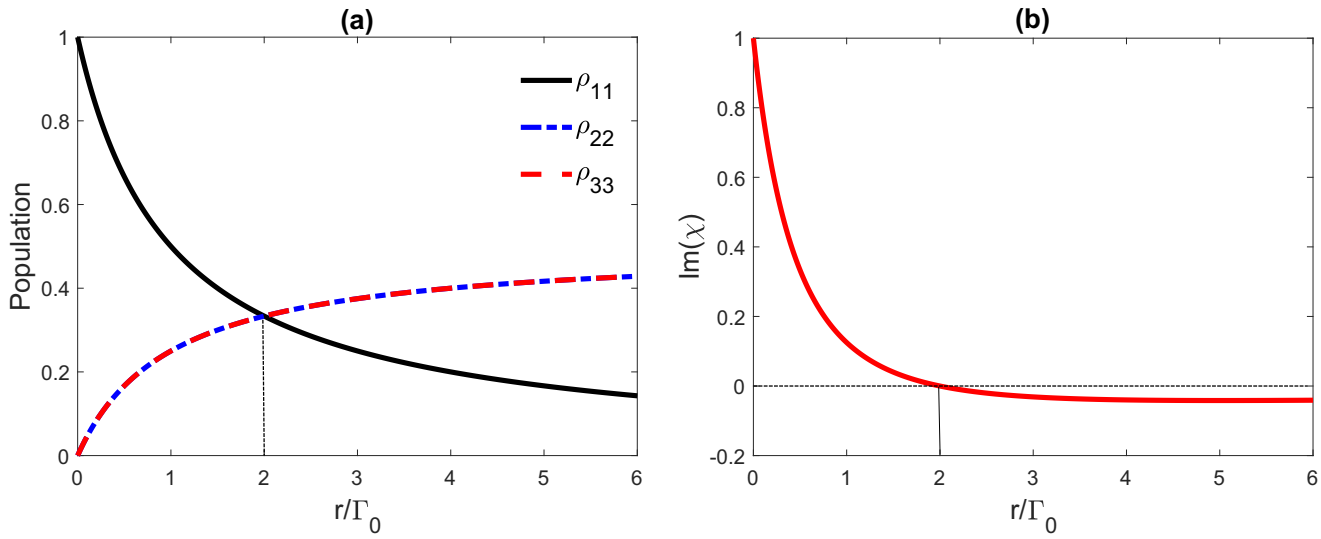

FIG. 6. (a) Population distributions ρ_{11}, ρ_{22}, and ρ_{33} and (b) the gain spectrum [Im(χ)] (in units of $\frac{N\mu^2}{\varepsilon_0\hbar}$) of the quantum V system as a function of the incoherent pumping r in the absence of plasmonic nanostructure. We have taken $\delta = 0$, $\omega_{32} = 0$. The quantum system is in the absence of plasmonic nanostructure ($d = \infty$). The horizontal dotted line indicates the zero-absorption limit, while the vertical dotted (solid) line indicates the threshold for the incoherent pumping to achieve the population inversion r_T^{PI} (gain r_T^L).

Im(χ) < 0. The susceptibility profiles are plotted in units of $\frac{N\mu^2}{\varepsilon_0\hbar}$. We assume in Figs. 2–10 that the dephasing rates are unimportant, and set $\gamma_{ij} = 0$. The effect of dephasing rates on the results will be studied in Fig. 11. In Fig. 2 we present the absorption-dispersion profiles against the probe detuning δ in the absence of incoherent pumping $r = 0$ and for the degenerate case corresponding to $E_2 = E_3$ and thus $\omega_{32} = 0$. Note that in all cases, we have selected distances where the influence of the plasmonic nanostructure varies significantly. Let us first consider the case where the quantum system is in the vacuum rather than in the plasmonic nanostructure. In this case the probe absorption is a sum of two independent Lorentzians with widths Γ_0 shown in Fig. 2(a). When the emitter is placed next to the plasmonic nanostructure while the distance of the quantum V system from the plasmonic nanostructure increases and gets closer to c/ω_p, very narrow resonances appear at the zero detuning; see Figs. 2(b)–2(d). In this case, the entire absorption spectrum is enhanced as $\Gamma_\perp$ and $\Gamma_\parallel$ decrease with distance. Moreover, the widths of absorption peaks are also reduced with $\Gamma_\perp$, leading to very sharp resonant absorption peaks. The slope of dispersion is always negative around the line center suggesting the occurrence of superluminal light propagation.

The absorption and dispersion properties are very different when the doublet splitting plays a role ($\omega_{32} \neq 0$). In Fig. 3, we present results when the quantum V system is near the plasmonic nanostructure, where we have set $\omega_{32} = \Gamma_0$ and $r = 0$ in the numerical simulations. Note that a transparency window appears at the center of the absorption spectrum around which the slope of dispersion changes to positive (slow light). The bigger is the distance of the quantum system to the plasmonic nanostructure, the deeper is the transparency window. Large enhancement of the refractive index is also observed, as the zero absorption is accompanied by a large dispersion for the largest distance $d = 0.9c/\omega_p$ [see the height of the dashed curve in Fig. 3(d)]. The width of the induced hole in the absorption profiles depends on the doublet splitting ω_{32}. We observe an increase of such a width with the splitting ω_{32}, leading to a wider window of transparency (see Fig. 4).

2. With incoherent pumping

Figures 2–4 illustrate that it is impossible for the probe field to be amplified when the incoherent pumping r is absent. The situation becomes quite different in the presence of r. The effect of incoherent pumping rate r on the absorption and dispersion spectra of the system is shown in Fig. 5 for the particular distance $d = 0.8c/\omega_p$ from the plasmonic nanostructure and when $\omega_{32} = \Gamma_0$. To begin with, we choose $r = 0.2\Gamma_0$. In Fig. 5(a) we display the absorption (solid curve) and dispersion (dashed curve) of the probe laser, respectively, as a function of the probe detuning δ. Comparing this figure with Fig. 3, one can see that a very weak incoherent pumping $r = 0.2\Gamma_0$ significantly reduces the absorption and dispersion heights. The probe field starts to experience gain on resonance for a larger incoherent pumping rate $r = 0.3\Gamma_0$ [Fig. 5(b)]. Moreover, the zero absorption for a nonresonant probe field on both sides of $\delta = 0$ is accompanied by an enhanced refractive index. The level of gain is altered by the rate of incoherent pumping. For example, further increasing the incoherent pumping to $r = 0.45\Gamma_0$ and $r = 0.6\Gamma_0$ enhances the probe gain, as one can see in Figs. 5(c) and 5(d). Such a gain is accompanied by the slow light around $\delta = 0$.

C. Gain with and without inversion

As shown in Fig. 5, the V system can exhibit the probe gain in the presence of an incoherent pumping. The gain can be with or without population inversion, depending on the distance to the plasmonic nanostructure and the strength of incoherent pump field. In what follows, we investigate the

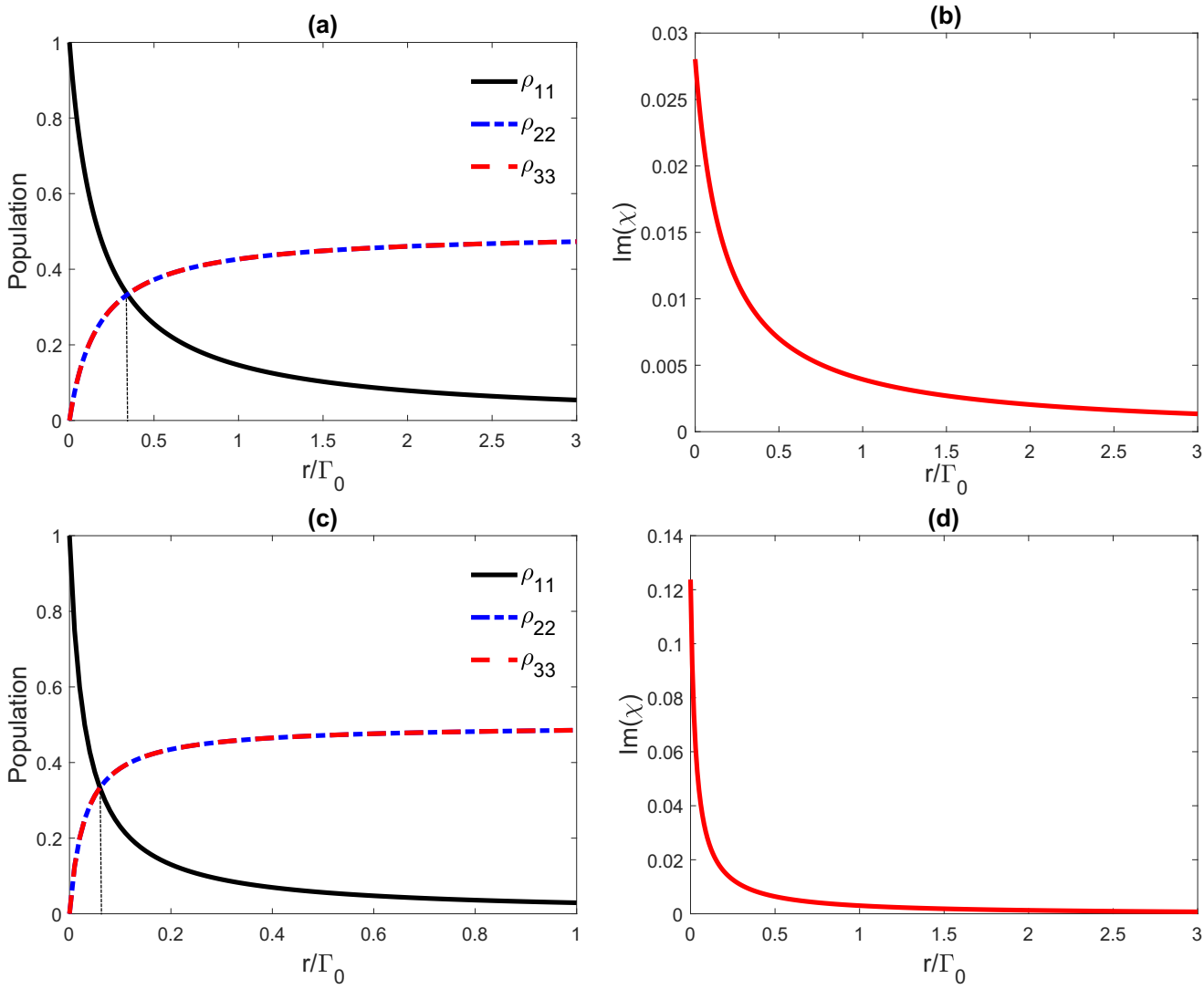

FIG. 7. (a), (c) Population distributions ρ_{11}, ρ_{22}, and ρ_{33} and (b), (d) the gain spectrum [Im(χ)] (in units of $\frac{N\mu^2}{\varepsilon_0\hbar}$) of the quantum V system as a function of the incoherent pumping r. We take here $\delta = 0$, $\omega_{32} = 0$, $\bar{\omega} = 0.632\omega_p$. The distances d of the quantum system from the plasmonic nanostructure are (a), (b) $d = 0.1c/\omega_p$ and (c), (d) $d = 0.3c/\omega_p$. The vertical dotted line indicates the threshold for the incoherent pumping to achieve the population inversion r_T^{PI}.

limits for the incoherent pumping to make gain with and without inversion, and discuss how the plasmonic nanostructure affects the results. Calling on Eqs. (5)–(7), one can obtain expressions for the population inversion as

$$\rho_{22} - \rho_{11} = \rho_{33} - \rho_{11} = \left(\frac{r}{2\gamma - \frac{8\gamma\kappa^2}{4\gamma^2+\omega_{32}^2}} - 1 \right) \rho_{11}. \quad (20)$$

This shows that the population differences $\rho_{22} - \rho_{11}$ and $\rho_{33} - \rho_{11}$ depend on the incoherent pumping rate r, as well as on the quantum interference described by κ which depends on the distance from the plasmonic nanostructure. Substituting Eqs. (10) and (11) into Eqs. (20), the threshold of incoherent pumping to achieve the population inversion can be expressed as

$$r_T^{PI} = (\Gamma_\perp + \Gamma_\parallel)\left[1 - \frac{\Gamma_\perp^2 + \Gamma_\parallel^2 - 2\Gamma_\perp\Gamma_\parallel}{\Gamma_\perp^2 + \Gamma_\parallel^2 + 2\Gamma_\perp\Gamma_\parallel + \omega_{32}^2} \right]. \quad (21)$$

Clearly, the population inversion is dominant if $r_T^{PI} > (\Gamma_\perp + \Gamma_\parallel) - \frac{(\Gamma_\perp+\Gamma_\parallel)(\Gamma_\perp^2+\Gamma_\parallel^2-2\Gamma_\perp\Gamma_\parallel)}{\Gamma_\perp^2+\Gamma_\parallel^2+2\Gamma_\perp\Gamma_\parallel+\omega_{32}^2}$; otherwise no inversion appears in the population distributions.

Let us now consider the situation where the plasmonic nanostructure is absent, which corresponds to the limit $d = \infty$. In this case, the second term is zero in the brackets on the right-hand side of Eq. (21), leading to the population inversion threshold for incoherent pumping:

$$r_T^{PI} = \Gamma_\perp + \Gamma_\parallel. \quad (22)$$

Equation (22) demonstrates that in the absence of plasmonic nanostructure, the population inversion is achieved only if the condition $r_T^{PI} > 2\Gamma_0$ is satisfied. This has been checked in Fig. 6(a) where we have depicted the distribution of populations against the incoherent pumping r. Putting $\delta = 0$, $\kappa = 0$, and $\omega_{32} = 0$ in Eqs. (17)–(20), the absorption coefficient in

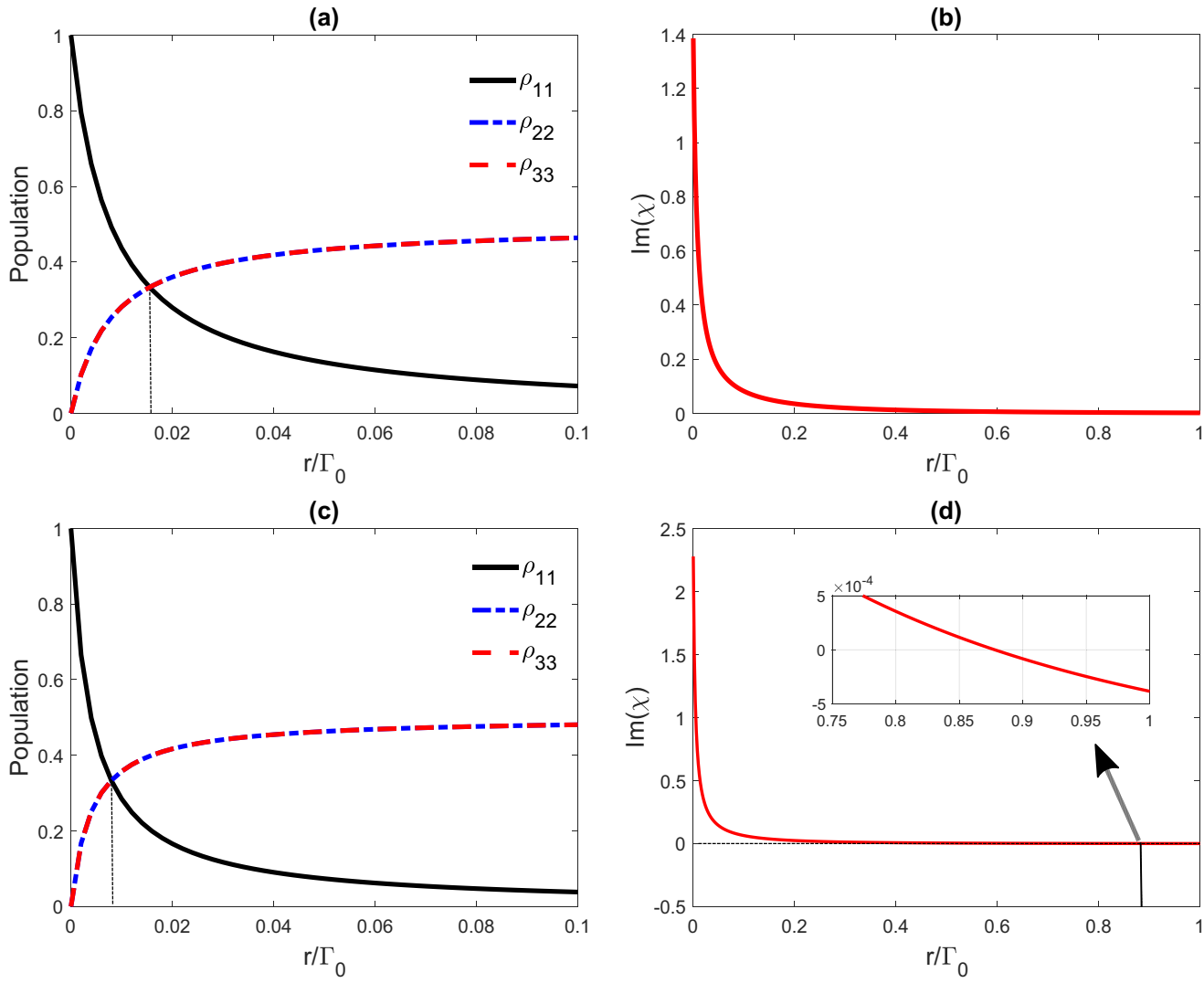

FIG. 8. (a), (c) Population distributions ρ_{11}, ρ_{22}, and ρ_{33} and (b), (d) the gain spectrum [Im(χ)] (in units of $\frac{N\mu^2}{\varepsilon_0\hbar}$) of the quantum V system as a function of the incoherent pumping r. We take here $\delta = 0$, $\omega_{32} = 0$, and $\bar{\omega} = 0.632\omega_p$. The distances d of the quantum system from the plasmonic nanostructure are (a), (b) $d = 0.7c/\omega_p$ and (c), (d) $d = 0.8c/\omega_p$. The horizontal dotted line indicates the zero-absorption limit, while the vertical dotted (solid) line indicates the threshold for the incoherent pumping to achieve the population inversion r_T^{PI} (gain r_T^L).

this case reads

$$\mathrm{Im}(\chi|_{\delta=0}) = -\frac{N\mu^2}{\varepsilon_0\hbar}\frac{\left(\frac{r}{\Gamma_\perp+\Gamma_\parallel}-1\right)}{\left[\frac{\Gamma_\perp}{2}+\frac{\Gamma_\parallel}{2}+r\right]}\rho_{11}. \tag{23}$$

Obviously, for $r = 0$ one has $\mathrm{Im}(\chi|_{\delta=0}) > 0$, so no gain appears in the system (see also Fig. 2). Equation (23) demonstrates also that in the absence of plasmonic nanostructure, the threshold for r to make the gain is

$$r_T^L = (\Gamma_\perp + \Gamma_\parallel), \tag{24}$$

which is the same as the one in Eq. (22) for the population inversion. Equations (22) and (24) imply that the gain is accompanied with population inversion in the region $r_T^{PI} = r_T^L > 2\Gamma_0$. This is more clearly shown in Fig. 6(b) where we plot the gain spectrum against the incoherent pumping. We find that no gain without population inversion is possible when the quantum system is far away from the plasmonic nanostructure ($d = \infty$).

Next, we turn our attention to the influence of the plasmonic nanostructure, while still keeping the assumption that $\delta = 0$ and $\omega_{32} = 0$. In this case, Eq. (21) reduces to

$$r_T^{PI} = (\Gamma_\perp + \Gamma_\parallel)\left[1 - \frac{\Gamma_\perp^2 + \Gamma_\parallel^2 - 2\Gamma_\perp\Gamma_\parallel}{\Gamma_\perp^2 + \Gamma_\parallel^2 + 2\Gamma_\perp\Gamma_\parallel}\right]. \tag{25}$$

The second term in brackets on the right-hand side of Eq. (25) is now nonzero, indicating that the plasmonic nanostructure facilitates the emergence of population inversion via reduction of the threshold r_T^{PI}. This is illustrated in Figs. 7 and 8, where we display the numerical results for the population distributions ρ_{11}, ρ_{22}, and ρ_{33} and the gain spectrum [Im(χ)] versus the incoherent pumping r for several values of d. In the presence of plasmonic nanostructure and for shorter distances $d = 0.1c/\omega_p$ and $d = 0.3c/\omega_p$ [see Figs. 7(a) and 7(c)], the threshold of the incoherent pump to acquire the population inversion is reduced remarkably as compared to the case when $d = \infty$ (compare with Fig. 6).

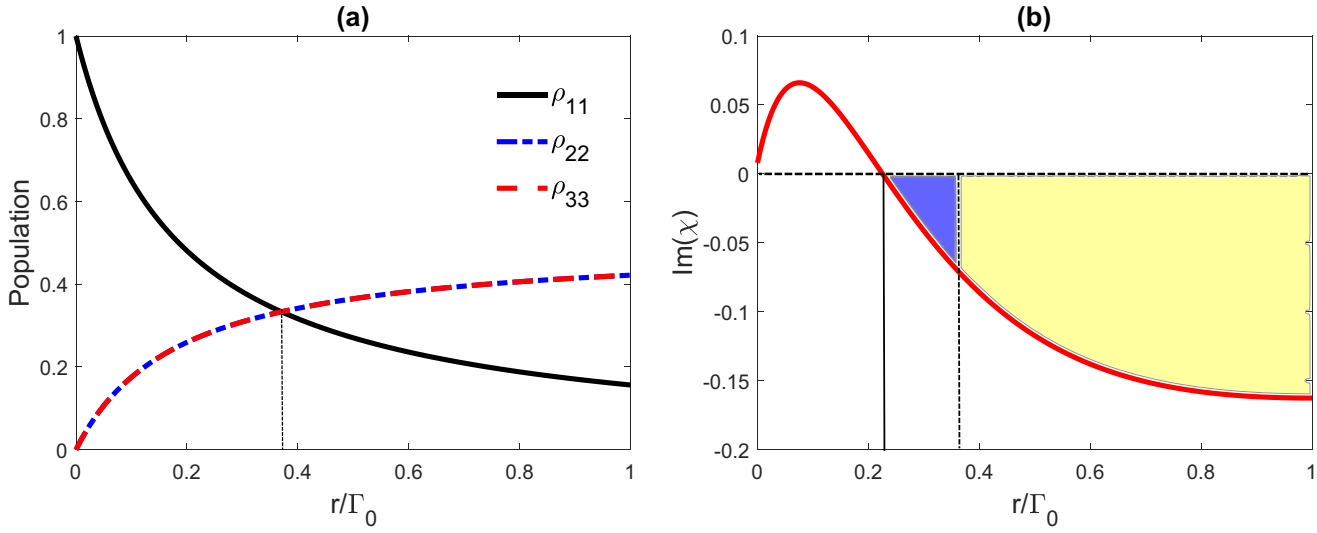

FIG. 9. (a) Population distributions ρ_{11}, ρ_{22}, and ρ_{33} and (b) the gain spectrum [Im(χ)] (in units of $\frac{N\mu^2}{\varepsilon_0\hbar}$) of the quantum V system as a function of the incoherent pumping r for $\delta = 0$, $\omega_{32} = \Gamma_0$, and $\bar{\omega} = 0.632\omega_p$. The distance d of the quantum system from the plasmonic nanostructure is $d = 0.8c/\omega_p$. The horizontal dashed line shows the zero-absorption limit; the vertical dotted (solid) line indicates the threshold for the incoherent pumping to achieve the population inversion r_T^{PI} (gain r_T^L). Gain without inversion appears for $r_T^L < r < r_T^{PI}$ [blue zone in Fig. 9(b)], while the gain with inversion takes place at $r > r_T^{PI}$ [yellow zone in Fig. 9(b)].

Obviously, the population inversion threshold r_T^{PI} for incoherent pumping is less than $0.5\Gamma_0$ for $d = 0.1c/\omega_p$ [Figs. 7(a)], while it approaches $0.1\Gamma_0$ when $d = 0.3c/\omega_p$ [Figs. 7(c)]. At this point we should stress that inclusion of the plasmonic nanostructure makes it almost impossible to determine the analytical limits for the gain threshold r_T^L, and the analytical solutions are quite complex and noninformative. Therefore, we present numerical results to identify the limits for the gain threshold r_T^L. According to Figs. 7(b) and 7(d) no gain is possible for the small distances of $d = 0.1c/\omega_p$ and $d = 0.3c/\omega_p$, so any population inversion is without the gain in such cases.

For larger distances d of the quantum system from the plasmonic nanostructure, the population inversion threshold for the incoherent pumping r_T^{PI} is even more reduced. For example, Fig. 8(a) illustrates that the threshold r_T^{PI} reduces to less than $0.02\Gamma_0$ for $d = 0.7c/\omega_p$, whereas the threshold r_T^{PI} is further reduced to less than $0.01\Gamma_0$ for $d = 0.8c/\omega_p$ [Fig. 8(c)]. For the latter case, the population inversion is accompanied by the gain for $r > 0.87\Gamma_0$ [see Fig. 8(d)]. Normally, in the presence of an incoherent pumping field, more population can be pumped and trapped in the excited levels $|2\rangle$ and $|3\rangle$ via the quantum interference in spontaneous emission, while, at the same time, less population is kept in the ground level $|1\rangle$. The degree of quantum interference can be controlled by changing the distance from the plasmonic nanostructure. For distances for which the quantum interference is maximum, high population inversion can be established on the transitions $|1\rangle \rightarrow |2\rangle$ and $|1\rangle \rightarrow |3\rangle$ even with a very weak incoherent pump rate. It should be pointed out that the induced gain is always accompanied by the population inversion in this case where $\omega_{32} = 0$.

From Eq. (21), it can be found that the population inversion threshold r_T^{PI} can also be modified and eventually increased by adjusting the splitting ω_{32}. In Fig. 9, we show the results of the population distributions and the gain spectrum at a particular distance $d = 0.8c/\omega_p$ of the quantum system from the plasmonic nanostructure for nonzero splitting for $\omega_{32} = \Gamma_0$. Here, the most interesting result is the emergence of two different regimes for the incoherent pumping: a region for the incoherent pumping $r > r_T^{PI}$ where the gain with the inversion appears [yellow zone in Fig. 9(b)], and a region $r_T^L < r < r_T^{PI}$ where the gain without the inversion takes place [blue zone in Fig. 9(b)]. One can see now that the value of incoherent pumping $r = 0.3\Gamma_0$ used to plot Fig. 5(b) lies in the blue region $r_T^L < r < r_T^{PI}$. This indicates that the gain in Fig. 5(b) is without the inversion. On the other hand, the resonant gain for $r = 0.45\Gamma_0$ and $r = 0.6\Gamma_0$ observed in Figs. 5(c) and 5(d) is now found to be with population inversion, as $r = 0.45\Gamma_0$ and $r = 0.6\Gamma_0$ are in the yellow zone $r > r_T^{PI}$.

The incoherent pumping region for achieving the gain with or without inversion can be controlled through different external parameters of the system: the distance of the quantum system from the plasmonic nanostructure and the splitting ω_{32}. As an example, in Fig. 10 we have depicted the results for two different distances (a), (b) $d = 0.8c/\omega_p$ and (c), (d) $d = c/\omega_p$ with the splitting taken to be $\omega_{32} = 1.5\Gamma_0$. It is apparent that for $d = 0.8c/\omega_p$ and $\omega_{32} = 1.5\Gamma_0$, the blue zone in Fig. 10(b) is wider than the one in Fig. 9(b), implying that the gain in the absence of population inversion can be obtained for a wider range of incoherent pumping. However, the region becomes narrower for $d = c/\omega_p$ and $\omega_{32} = 1.5\Gamma_0$, which suggests that the induced gain without inversion occurs for a smaller range of incoherent pumping as compared to the situation shown in Fig. 9(b).

Finally, we consider in Fig. 11 the influence of dephasing rates γ_{ij} on the results. We consider the case in which the distance to the plasmonic nanostructure is $d = 0.8c/\omega_p$. We assume $\gamma_{21} = \gamma_{31} = \gamma_{23} = 0.5\Gamma_0$ and set the other parameters the same as Fig. 10. Clearly, the absorption (gain) of the

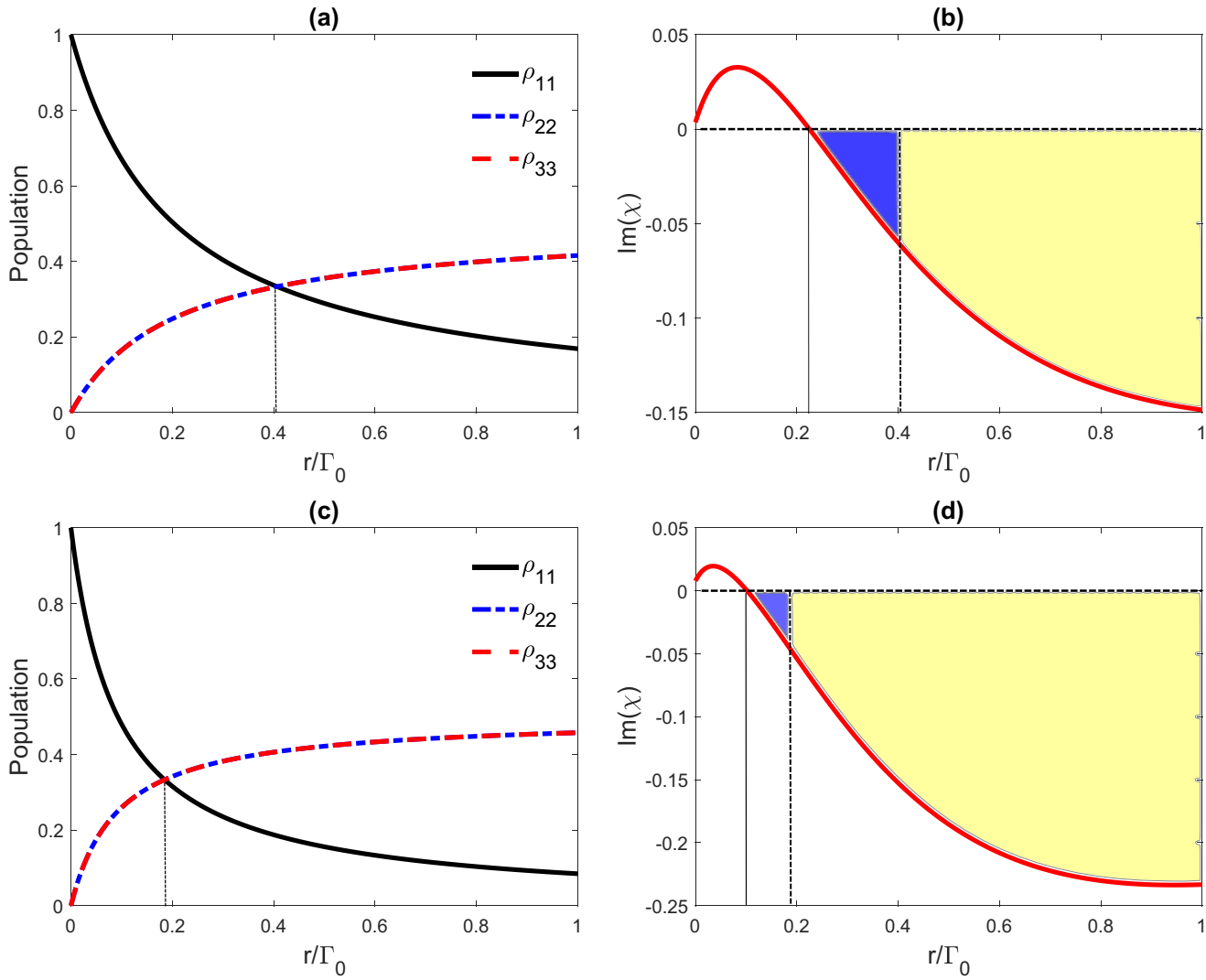

FIG. 10. (a), (c) Population distributions ρ_{11}, ρ_{22}, and ρ_{33} and (b), (d) the gain spectrum [Im(χ)] (in units of $\frac{N\mu^2}{\varepsilon_0\hbar}$) of the quantum V system as a function of the incoherent pumping r for $\delta = 0$, $\omega_{32} = 1.5\Gamma_0$, and $\bar{\omega} = 0.632\omega_p$. The distances d of the quantum system from the plasmonic nanostructure are (a), (b) $d = 0.8c/\omega_p$ and (c), (d) $d = c/\omega_p$. The horizontal dashed line shows the zero-absorption limit; the vertical dotted (solid) line indicates the threshold for the incoherent pumping to achieve the population inversion r_T^{PI} (gain r_T^L). Gain without inversion appears for $r_T^L < r < r_T^{PI}$ [blue zones in panels (b) and (d)], while the gain with inversion takes place at $r > r_T^{PI}$ [yellow zones in panels (b) and (d)].

medium is increased now [compared with Fig. 10(b)], leading to a smaller range of incoherent pumping in which the gain without inversion is established [compare blue zones in Figs. 10(b) and 11(b)]. This is due to the partial destruction of quantum coherence in the presence of dephasing rates.

Before closing, we note that the gain without inversion in this work is not related to strong-coupling effects, as for example happens with the work of "thresholdless" lasers in the literature [65]. The gain without inversion occurs when the quantum system is in the proximity of the plasmonic nanostructure but the interaction happens in the weak-coupling regime, where the Purcell effect changes the spontaneous decay rate. The asymmetric change in the spontaneous decay rates for orthogonal electric dipoles leads to quantum interference in spontaneous emission, which in turn leads to gain without inversion similar to the ideas of Harris [40]. What happens is that the presence of quantum interference breaks the symmetry between absorption and emission, and while absorption in the system shows a minimum (transparency), the emission occurs regularly and shows a maximum at the spectra region of minimum absorption.

IV. CONCLUDING REMARKS

In summary, we have studied the absorption and dispersion properties of a three-level V-type quantum system with a closely spaced doublet, interacting with a weak probe field. The response of such a quantum V-type system is influenced by a nearby lattice of plasmonic nanostructure, a 2D array of metal-coated dielectric nanospheres (plasmonic nanoshells). The plasmonic nanostructure modifies drastically the decay rates which have been calculated by an electromagnetic Green's tensor technique [3]. We have shown a remarkable modification of optical properties of the quantum

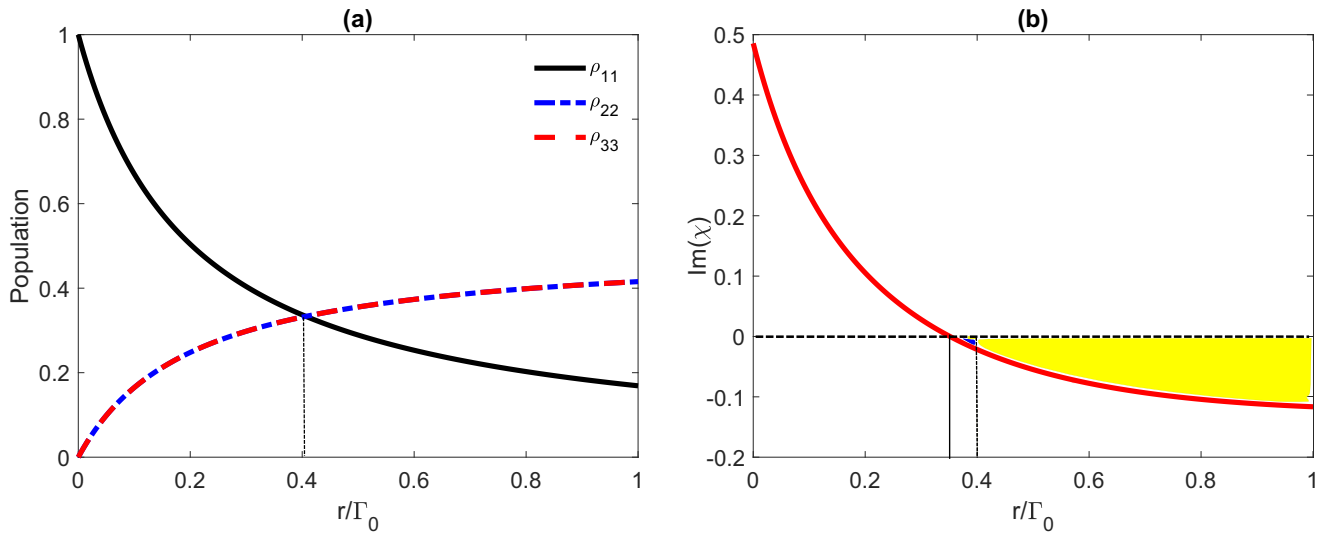

FIG. 11. (a) Population distributions ρ_{11}, ρ_{22}, and ρ_{33} and (b) the gain spectrum [Im(χ)] (in units of $\frac{N\mu^2}{\varepsilon_0\hbar}$) of the quantum V system as a function of the incoherent pumping r. The distance d of the quantum system from the plasmonic nanostructure is $d = 0.8c/\omega_p$. The parameters are the same as Fig. 10, but now $\gamma_{21} = \gamma_{31} = \gamma_{23} = 0.5\Gamma_0$. The horizontal dashed line shows the zero-absorption limit; the vertical dotted (solid) line indicates the threshold for the incoherent pumping to achieve the population inversion r_T^{PI} (gain r_T^L). Gain without inversion appears for $r_T^L < r < r_T^{PI}$ [blue zone in panel (b)], while the gain with inversion takes place at $r > r_T^{PI}$ [yellow zone in panel (b)].

V-type system when placed next to the plasmonic nanostructure. Namely, depending upon the values of doublet splitting, either very narrow resonances or optical transparency can be realized for a weak probe field. Applying an incoherent pumping field, the absorption effects are further modified, yielding probe gain (with or without population inversion). Such a gain is shown to be tuned by modifying the distance of the quantum system from the plasmonic nanostructure, the incoherent pumping rate, and the doublet splitting. We have analytically and numerically determined threshold limits for the incoherent pumping for which the induced gain is with or without the population inversion.

It should be pointed out that the inversionless gain demonstrated here is achieved without any strong coherent pump field. The phenomenon is quite different from the one realized in a double-V quantum scheme near a plasmonic nanostructure, where a coherent pump field is applied to create the coherence and provide the gain [34]. Compared to this double-V-type configuration, a single-V-type quantum system is much easier to implement with atoms, molecules, and quantum dots. The inversionless gain mechanism proposed here is also different from conventional methods [40–46], because it is achieved by means of a plasmonic nanostrucuture.

This work may lead to new horizons in controllable nanoplasmonics devices [66–68] for quantum optical applications down to a single plasmon level, extending the domain of quantum coherence and interference beyond its conventional platform of atomic, molecular, and optical physics.

ACKNOWLEDGMENTS

This project has received funding from the European Social Fund (Project No. 09.3.3-LMT-K-712-19-0031) under a Grant Agreement with the Research Council of Lithuania (LMTLT) for H.R.H.

[1] B. Szychowski, M. Pelton, and M. C. Daniel, Nanophotonics **8**, 517 (2019).
[2] Y. V. Vladimirova and V. N. Zadkov, Nanomaterials **11**, 1919 (2021).
[3] V. Yannopapas, E. Paspalakis, and N. V. Vitanov, Phys. Rev. Lett. **103**, 063602 (2009)
[4] Y. Gu, L. Wang, P. Ren, J. Zhang, T. Zhang, O. J. F. Martin, and Q. Gong, Nano Lett. **12**, 2488 (2012).
[5] C. Sanchez-Munoz, A. Gonzalez-Tudela, and C. Tejedor, Phys. Rev. B **85**, 125301 (2012).
[6] R.-C. Ge, C. Van Vlack, P. Yao, J. F. Young, and S. Hughes, Phys. Rev. B **87**, 205425 (2013).
[7] J. Hakami, L. Wang, and M. S. Zubairy, Phys. Rev. A **89**, 053835 (2014).
[8] D.-X. Zhao, Phys. Rev. A **98**, 033834 (2018).
[9] A. Mohammadzadeh and M. Miri, Phys. Rev. B **99**, 115440 (2019).
[10] S. Shen, Z.-M. Wu, J.-H. Li, and Y. Wu, Phys. Rev. A **104**, 013717 (2021).
[11] S. Evangelou, V. Yannopapas, and E. Paspalakis, Phys. Rev. A **86**, 053811 (2012).
[12] E. Paspalakis, S. Evangelou, V. Yannopapas, and A. F. Terzis, Phys. Rev. A **88**, 053832 (2013).
[13] L. Wang, Y. Gu, H. Chen, J.-Y. Zhang, Y. Cui, B. Gerardot, and Q.-H. Gong, Sci. Rep. **3**, 2879 (2013).
[14] J.-H. Li, S. Shen, C.-L. Ding, and Y. Wu, Phys. Rev. A **103**, 053706 (2021).
[15] Z.-P. Wang and B.-L. Yu, Plasmonics **13**, 567 (2018).

[16] B. S. Nugroho, A. A. Iskandar, V. A. Malyshev, and J. Knoester, Phys. Rev. B **102**, 045405 (2020).

[17] R. D. Artuso and G. W. Bryant, Phys. Rev. B **82**, 195419 (2010).

[18] W. Zhang, A. O. Govorov, and G. W. Bryant, Phys. Rev. Lett. **97**, 146804 (2006).

[19] M. R. Singh, D. G. Schindel, and A. Hatef, Appl. Phys. Lett. **99**, 181106 (2011).

[20] H. Hapuarachchi, S. D. Gunapala, Q. Bao, M. I. Stockman, and M. Premaratne, Phys. Rev. B **98**, 115430 (2018).

[21] A. V. Malyshev and V. A. Malyshev, Phys. Rev. B **84**, 035314 (2011).

[22] B. S. Nugroho, V. A. Malyshev, and J. Knoester, Phys. Rev. B **92**, 165432 (2015).

[23] G. Solookinejad, M. Jabbari, M. Nafar, E. Ahmadi, and S. H. Asadpour, J. Appl. Phys. **124**, 063102 (2018).

[24] H. Chen, J. Ren, Y. Gu, D. Zhao, J. Zhang, and Q. Gong, Sci. Rep. **5**, 18315 (2016).

[25] X. Liu, N. Kongsuwan, X.-G. Li, D.-X. Zhao, Z.-M. Wu, O. Hess, and X.-H. Zhang, J. Phys. Chem. Lett. **10**, 7594 (2019).

[26] H. R. Hamedi, V. Yannopapas, A. Mekys, and E. Paspalakis, Phys. E **130**, 114662 (2021).

[27] J.-B. Li, N.-C. Kim, M.-T. Cheng, L. Zhou, Z.-H. Hao, and Q.-Q. Wang, Opt. Express **20**, 1856 (2012).

[28] S. K. Singh, M. K. Abak, and M. E. Tasgin, Phys. Rev. B **93**, 035410 (2016).

[29] A. Vafafard, M. Sahrai, S. H. Asadpour, and E. Faizabadi, J. Opt. Soc. Am. B **38**, 1892 (2021).

[30] S. M. Sadeghi, Nanotechnology **21**, 455401 (2010).

[31] S. G. Kosionis, A. F. Terzis, S. M. Sadeghi, and E. Paspalakis, J. Phys.: Condens. Matter **25**, 045304 (2013).

[32] S. M. Sadeghi, Phys. Rev. A **88**, 013831 (2013).

[33] D. Zhao, Y. Gu, J. Wu, J. Zhang, T. Zhang, B. D. Gerardot, and Q. Gong, Phys. Rev. B **89**, 245433 (2014).

[34] F. Carreño, M. A. Antón, V. Yannopapas, and E. Paspalakis, Phys. Rev. B **95**, 195410 (2017).

[35] S. H. Asadpour and M. Jafari, Opt. Commun. **421**, 125 (2018).

[36] Y. You, Y. H. Qi, Y.-P. Niu, and S.-Q. Gong, J. Phys.: Condens. Matter **31**, 105801 (2019).

[37] S. Evangelou, Microelectron. Eng. **215**, 111019 (2019).

[38] M. R. Singh, Nanotechnology **24**, 125701 (2013).

[39] P. K. Jha, Y. Wang, X. Ren, and X. Zhang, J. Opt. **19**, 054002 (2017).

[40] S. E. Harris, Phys. Rev. Lett. **62**, 1033 (1989).

[41] Y. Zhu, Phys. Rev. A **45**, R6149 (1992).

[42] M. O. Scully, S.-Y. Zhu, and A. Gavrielides, Phys. Rev. Lett. **62**, 2813 (1989).

[43] W.-H. Xu, J.-H. Wu, and J.-Y. Gao, J. Phys. B: At. Mol. Opt. Phys. **39**, 1461 (2006).

[44] A. A. Svidzinsky, L. Yuan, and M. O. Scully, New J. Phys. **15**, 053044 (2013).

[45] O. Kocharovskaya, A. B. Matsko, and Y. Rostovtsev, Phys. Rev. A **65**, 013803 (2001).

[46] J.-H. Wu, Zheng-Lin Yu, and J.-Y. Gao, Opt. Commun. **211**, 257 (2002).

[47] V. V. Kozlov, Y. Rostovtsev, and M. O. Scully, Phys. Rev. A **74**, 063829 (2006).

[48] G. S. Agarwal, Phys. Rev. Lett. **84**, 5500 (2000).

[49] M. Kiffner, M. Macovei, J. Evers, and C. H. Keitel, Prog. Opt. **55**, 85 (2010).

[50] Y. Yang, J. Xu, H. Chen, and S. Zhu, Phys. Rev. Lett. **100**, 043601 (2008).

[51] G.-x. Li, J. Evers, and C. H. Keitel, Phys. Rev. B **80**, 045102 (2009).

[52] P. K. Jha, X. Ni, C. Wu, Y. Wang, and X. Zhang, Phys. Rev. Lett. **115**, 025501 (2015).

[53] S. Hughes and G. S. Agarwal, Phys. Rev. Lett. **118**, 063601 (2017).

[54] S. Zhang, W. Ni, X. Kou, M. H. Yeung, L. Sun, J. Wang, and C. Yan, Adv. Funct. Mater. **17**, 3258 (2007).

[55] J. Liu, H. Dong, Y. Li, P. Zhan, M. Zhu, and Z. Wang, Jpn. J. Appl. Phys. **45**, L582 (2006).

[56] S. Yang, W. Cai, L. Kong, and Y. Lei, Adv. Funct. Mater. **20**, 2527 (2010).

[57] R. B. Johnson and R. W. Christy, Phys. Rev. B **6**, 4370 (1972).

[58] M. M. Wind, P. A. Bobbert, J. Vlieger, and D. Bedeaux, Physica A **143**, 164 (1987).

[59] P. A. Bobbert and J. Vlieger, Physica A **147**, 115 (1987).

[60] R. Sainidou, N. Stefanou, and A. Modinos, Phys. Rev. B **69**, 064301 (2004).

[61] V. Yannopapas and N. V. Vitanov, Phys. Rev. B **75**, 115124 (2007).

[62] N. Stefanou, V. Yannopapas, and A. Modinos, Comput. Phys. Commun. **113**, 49 (1998).

[63] N. Stefanou, V. Yannopapas, and A. Modinos, Comput. Phys. Commun. **132**, 189 (2000).

[64] V. Yannopapas, J. Opt. Soc. Am. B **31**, 631 (2014).

[65] M. Khajavikhan, A. Simic, M. Katz, J. H. Lee, B. Slutsky, A. Mizrahi, V. Lomakin, and Y. Fainman, Nature (London) **482**, 204 (2012).

[66] Z. Jacob and V. M. Shalaev, Science **334**, 463 (2011).

[67] M. S. Tame, K. R. McEnery, S. K. Ozdemir, J. Lee, S. A. Maier, and M. S. Kim, Nat. Phys. **9**, 329 (2013).

[68] P. K. Jha, M. Mrejen, J. Kim, C. Wu, X. Yin, Y. Wang, and X. Zhang, Appl. Phys. Lett. **105**, 111109 (2014).